miR-126 regulates glycogen trophoblast proliferation and DNA methylation in the murine placenta

Abhijeet Sharma[a,#], **Lauretta A. Lacko**[a,b], **Lissenya B. Argueta**[a], **Michael D. Glendinning**[a], and **Heidi Stuhlmann**[a,*]

[a]Department of Cell and Developmental Biology, Weill Cornell Medical College, 1300 York Avenue, Box 60, New York, NY 10065

[b]Department of Surgery, Weill Cornell Medical College, 1300 York Avenue, Box 60, New York, NY 10065

Abstract

A functional placenta develops through a delicate interplay of its vascular and trophoblast compartments. We have identified a previously unknown expression domain for the endothelial-specific microRNA *miR-126* in trophoblasts of murine and human placentas. Here, we determine the role of *miR-126* in placental development using a mouse model with a targeted deletion of *miR-126*. In addition to vascular defects observed only in the embryo, loss of *miR-126 function* in the placenta leads to junctional zone hyperplasia at E15.5 at the expense of the labyrinth, reduced placental volume for nutrient exchange and intra-uterine growth restriction of the embryos. Junctional zone hyperplasia results from increased numbers of proliferating glycogen trophoblast (GlyT) progenitors at E13.5 that give rise to an expanded glycogen trophoblast population at E15.5. Transcriptomic profile of *miR-126*$^{-/-}$ placentas revealed dysregulation of a large number of GlyT (*Prl6a1*, *Prl7c1*, *Pcdh12*) and trophoblast-specific genes (*Tpbpa*, *Tpbpb*, *Prld1*) and genes with known roles in placental development. We show that *miR-126*$^{-/-}$ placentas, but not *miR-126*$^{-/-}$ embryos, display aberrant expression of imprinted genes with important roles in glycogen trophoblasts and junctional zone development, including *Igf2, H19, Cdkn1c* and *Phlda2*, during mid-gestation. We also show that *miR126*$^{-/-}$ placentas display global hypermethylation, including at several imprint control centers. Our findings uncover a novel role for *miR-126* in regulating extra-embryonic energy stores, expression of imprinted genes and DNA methylation in the placenta.

[*]Corresponding Author: Heidi Stuhlmann, Ph.D., Department of Cell and Developmental Biology, Weill Cornell Medical College, 1300 York Avenue, Box 60, New York, NY 10065, Telephone: 212-746-6156, Fax: 212-746-8175, hes2011@med.cornell.edu.
[#]Present address: Department of Neurology, Icahn School of Medicine at Mount Sinai, 1 Gustave L. Levy Place, New York, NY 10029

Summary

The microRNA *miR-126* plays a critical role in placental development, affecting extra-embryonic energy stores, expression of imprinted genes, DNA methylation and embryonic growth.

Keywords

miR-126; Placenta; Glycogen trophoblasts; DNA methylation; Genomic imprinting

Introduction

The placenta is critical for the development and survival of the mammalian embryo. It is responsible for nutrient, gas and waste exchange, as well as immunological and endocrine functions critical during pregnancy (Watson and Cross, 2005). The murine placenta develops from two major lineages, the trophectoderm and the extraembryonic mesoderm (Rossant and Cross, 2001). The extraembryonic mesoderm forms the allantois and the mesothelium lining the chorionic ectoderm. After fusing with the chorion, the allantois gives rise to the vascular compartment of the fetal labyrinth. Trophectoderm cells invade and differentiate into a variety of trophoblast subtypes with diverse functions. In the labyrinth, syncytiotrophoblasts control transport of nutrients from maternal blood to fetal vessels (Watson and Cross, 2005), and sinusoidal trophoblast giant cells act as hematopoietic signaling centers (Chhabra et al., 2012). In the junctional zone, spongiotrophoblasts and trophoblast giant cells secrete progesterone, lactogens and prolactin-like hormones critical for maternal physiology. Junctional zone glycogen trophoblasts secrete IGF2 and store glycogen (Rossant and Cross, 2001; Watson and Cross, 2005). Defects in trophoblast development can lead to abnormal placentation with adverse consequences for the mother and the fetus. Placental pathologies like pre-eclampsia and intra uterine growth restriction can lead to embryonic demise (Rossant and Cross, 2001).

A number of genetic and epigenetic determinants control trophoblast differentiation and placental development (Lefebvre, 2012; Maltepe et al., 2010). Genomic imprinting is an epigenetic modification that regulates gene expression from a single allele based on parental origin (Plasschaert and Bartolomei, 2014). Allele specific DNA methylation at imprint control centers (ICRs) maintains monoallelic expression of imprinted genes (Barlow and Bartolomei, 2014). The importance of maintaining genomic imprints for placental development is highlighted in murine models where imprinted gene deletions and uniparental duplications result in placental abnormalities (Esquiliano et al., 2009; Georgiades et al., 2001; Lopez et al., 1996; Oh-McGinnis et al., 2011; Tunster et al., 2010). Human infants with naturally occurring imprinting disorders like Beckwith–Wiedemann and Silver-Russell syndromes have abnormal placentas (Gicquel et al., 2005; Maher and Reik, 2000; Schonherr et al., 2007). Genomic imprinting also affects nutrient availability and tissue development in utero (Green et al., 2015; Tunster et al., 2013). Interestingly, several known regulators of junctional zone trophoblast development are imprinted genes that are located in the *Igf2* and *Kcnq1ot1* clusters on the distal end of chromosome 7 in mice, including *Igf2*, *Cdkn1c*, *Phlda2*, and *Ascl2* (Cleaton et al., 2014; Ferguson-Smith et al., 2001; Lefebvre, 2012).

A recent study revealed a novel expression domain for the endothelial specific gene *Egfl7* in the trophectoderm and in trophoblasts of the placenta (Lacko et al., 2014). *miR-126*, a microRNA (miRNA) embedded in intron 7 of *Egfl7*, shares upstream regulatory elements with *Egfl7* (Wang et al., 2008). Embryos deficient in *miR-126* display vascular leakage, hemorrhaging, and partial embryonic lethality (Wang et al., 2008). The vascular defects can be attributed to diminished sprouting and adhesion of endothelial cells resulting from reduced angiogenic growth factor signaling. Studies in zebrafish and mice revealed that *miR-126* modulates developmental angiogenesis by post-transcriptionally regulating gene expression of inhibitors of growth factor induced AKT and ERK signaling (Fish et al., 2008; Wang et al., 2008). However, the expression of *miR-126* in the placenta and its function during placental development has not been investigated.

Here, we examine the role of *miR-126* in placental development using a *miR-126$^{-/-}$* mouse model (Wang et al., 2008). We show, for the first time, that *miR-126* controls proliferation of glycogen trophoblasts by regulating DNA methylation and expression of imprinted genes in the placenta.

Materials and Methods

Mice and genotyping

All animal protocols were approved and are in accordance with the Institutional Animal Care and Use Committee (IACUC) at Weill Cornell Medical College of Cornell University. *miR-126$^{+/-}$* mice (Wang et al., 2008) in a mixed genetic background were obtained from Dr. Eric Olsen (UT Southwestern Medical Center) and backcrossed for 10 generations into a congenic C57Bl6/J background. Genotyping was done by genomic PCR on DNA from yolk sac or tail biopsies, using the following primers: *mir-126* wild type-forward: 5'-GGGCCACTTTACCCTGAAGAG –3'; *miR-126* wild type-reverse: 5'-GCTGACCGCGCATTATTACTC-3'; *miR-126* floxed-reverse: 5' –GACGGTATCGATAAAGCTAGC-3'. For timed pregnancies, the day of a vaginal plug was designated as embryonic day 0.5. All experimental embryos and placentas were isolated from litters of *miR-126$^{+/-}$* × *miR-126$^{+/-}$* crosses. Embryonic sizes were calculated by crown to rump length measurements and placental sizes were calculated by measurements along the diameter of the placenta. Sex was determined by PCR of genomic DNA for *Jarid1* and *SRY* using the following primers:

Jarid1d-forward: 5' – CTGAAGCTTTTGGCTTTGAG – 3'

Jarid1d-reverse: 5' – CCACTGCCAAATTCTTTGG – 3'

SRY-forward: 5' – GAGAGCATGGAGGGCCATG – 3'

SRY-reverse: 5' – GAGTACAGGTGTGCAGC – 3'

In situ hybridization

In situ hybridization was performed as previously described (Nielsen, 2012). Briefly, OCT embedded mouse and human placenta sections were post-fixed with 4% PFA for 10mins and

washed with PBS. Slides were treated with an acetylation solution (500μl 6N HCl, 670μl triethanolamine, 300μl acetic anhydride in 48.5ml DEPC-treated water) for 5min at RT. Sections were pre-hybridized in hybridization buffer (50% formamide, 5× SSC, 500μg/μl yeast tRNA, 5mM EDTA, 1X Denhardt' solution) for 4hr at 55°C, and incubated with a DIG-labeled LNA *miR-126* LNA probe (Exiqon), or a DIG-labeled LNA scrambled probe overnight at 55°C. Slides were washed twice with 0.1× SSC at 60°C and 4 times with 2× SSC at RT, blocked for 1hr using a blocking buffer (10% blocking reagent, 20% heat inactivated goat serum in MABT) and incubated overnight at 4°C with alkaline phosphatase-conjugated anti-DIG antibody (1:1600, Roche). Sections were washed with MABT and NTMT (100 mM NaCl, 100 mM Tris–HCl pH9.5, 50 mM $MgCl_2$, 1% Tween20, 20 μM Levamisole, in H_2O). Signal was detected using NBT-BCIP (Roche) at RT. Sections were post-fixed in 4% paraformaldehyde and imaged using an Axioplan 2 imaging microscope (Carl Zeiss) with 20X and 40X objectives.

Derivation and culture of trophoblast stem cells (TSC)

$miR-126^{+/+}$ and $miR-126^{-/-}$ TSCs were derived from blastocyst of $miR-126^{+/-}$ intercrosses, as previously described (Tanaka et al., 1998). TSCs were grown in RPMI medium containing 20% FBS, 1mM sodium pyruvate, 50μg/ml penicillin/streptomycin, β-mercaptoethanol, 25ng/ml basic fibroblast growth factor (Biolegend) and 1μg/ml heparin (Invitrogen), with 70% conditioned medium from irradiated embryonic fibroblasts as previously described (Tanaka et al., 1998).

Histology and Immunohistochemistry

Placentas were isolated in ice-cold PBS, fixed in 4% paraformaldehyde overnight, and embedded in an OCT:30% sucrose mixture. Cryosections were permeabilized in 0.5% Triton-X/0.1% Saponin/PBS (TSP) and blocked with 1% donkey serum in 0.1% TSP/PBS (PBS–TSP). Sections were incubated overnight at 4°C with primary antibodies - CD31 (BD Biosciences, 553370, 5μg/ml); ENDOMUCIN (Santa Cruz, sc-65495, 20μg/ml); CYTOKERATIN (DAKO Z0622, 10μg/ml); TPBPA (Abcam, ab104401, 10μg/μl); p57/CDKN1C (Santa Cruz, sc-1039, 20μg/μl); ERG (Abcam, ab110639, 0.17μg/ml)-, followed by incubation with secondary antibodies (Alexa488-donkey-ɑ-rat, Alexa488-donkey-ɑ-rabbit, Alexa488-donkey-ɑ-goat and Alexa594-donkey-ɑ-rabbit, Jackson Immunoresearch, 1.5 μg/ml), and mounted with Prolong Gold + DAPI. Images were acquired using an Axioplan 2 imaging microscope with 20X and 40X objectives.

Measurement of labyrinth and junctional zone areas

Labyrinth and junctional zone areas were quantified from 6 images each of CD31 and TPBPA immunostained cryosections from $miR-126^{+/+}$ (n=6) and $miR-126^{-/-}$ (n=5) placentas derived from at least two litters of $miR-126^{+/-} \times miR-126^{+/-}$ crosses. The area stained positive for CD31 was quantified as the fetal labyrinth area, and the area stained positive for TPBPA was quantified as the junctional zone area. Labyrinth and junctional zone regions were traced using ImageJ software, and the percentage area was quantified.

EdU Labeling

Proliferating cells were labeled using the Click-iT EdU Imaging Kit (Life Technologies, C10339), as previously described (Lacko et al., 2017). Briefly, pregnant female *miR-126⁺/⁻* mice were subjected to intraperitoneal injection of EdU at 50 μg per gram of body weight at day 13.5 and day 15.5 of gestation. After 60 minutes, mice were euthanized and placentas were isolated and fixed in 4% paraformaldehyde overnight. Tissue was embedded in an OCT:30% sucrose mixture and sectioned for further processing. EdU detection was carried out according to the manufacturer's protocol. Antibody staining was then performed as described above. Approximately every 10th section was used for quantification of labeling, for a total of four sections per placenta (n=4 per genotype), and analyzed using ImageJ, Metamorph (Molecular Devices) and Prism (GraphPad) software.

Cell counts

Glycogen trophoblast and proliferating cells were quantified from 10–15 high magnification images of *miR-126⁺/⁺* (n=4) and *miR-126⁻/⁻* (n=4) immunostained placentas from at least two litters of *miR-126⁺/⁻ × miR-126⁺/⁻* crosses. CDKN1C⁺ TPBPA⁺ cells in the junctional zone of E13.5 and E15.5 placentas and EdU⁺CDKN1C⁺ TPBPA⁺ cells in the junctional zone of E13.5 were quantified using MetaMorph imaging software. Trophoblast giant cells were excluded based on the size of their nuclei.

Quantification of total glycogen from placental tissue

Total glycogen content in placentas was measured using previously described methods (Kemp and Van Heijningen, 1954). Briefly, placentas were weighed, and boiled for 20 min in a 30% KOH solution saturated with Na_2SO_4. After cooling on ice, glycogen was precipitated by adding 1.2 volumes of 95% ethanol. Samples were spun at 1000xg for 30min at 4°C, and the glycogen pellet was dissolved in ddH20. A phenol-sulfuric acid colorimetric method was used to determine glycogen content (Kemp and Van Heijningen, 1954).

Real Time RT-PCR

Embryos and decidua-free placentas (E12.5) were isolated in cold PBS and flash frozen in liquid nitrogen. RNA was isolated using Trizol (Invitrogen) and reverse transcribed using SuperScript II (Quanta Biosciences). Gene expression was measured quantitatively using PerfeCTa SYBR Green SuperMix for iQ (Quanta Biosciences). Primer sets are listed in the table shown below. Differences among target expression were quantified using the   CT method and normalized to ß-actin and 18S rRNA.

Gene	Forward Primer (5' –> 3')	Reverse primer (5' –> 3)
Igf2	AGCAATCGGAAGTGAGCAAAC	GGATGGAACCTGATGGAAACG
H19	GGCTCCCAGAACCCACAAC	GGGTTTTGTGTCCGGATTCA
Cdkn1c	GCCGGGTGATGAGCTGGGAA	AGAGAGGCTGGTCCTTCAGC
Phlda2	CCCGCCAAGGAGCTGTTT	CCTTGTAATAGTTGGTGACGATGGT
Kcnq1	CAAAGACCGTGGCAGTAAC	CCTTCATTGCTGGCTACAAC

Gene	Forward Primer (5' –> 3')	Reverse primer (5' –> 3)
Kcnq1ot1	GGTCTGAGGTAGGGATCAGG	GGCACACGGTATGAGAAAAGATTG
Grb10	AGGATCATCAAGCAACAAGGTCTC	ATTACTCTGGCTGTCACGAAGGA
Peg3	ATGCCCACTCCGTCAGCG	GCTCATCCTTGTGAACTTTG
Prl6a1	GGTCATTTCCCAGATGCTGT	GGGCTCCCTCCTTAGACACT
Prl7c1	CACATTTTCCCTCAGTGTTCCAGAA	GCACCTTTCATACAGTGGAGTTCAG
Pcdh12	CTCCTGTCCAGCAAATCTCC	TCTGCTTGACCACTAGGCTTG

For analysis of *miR-126* expression, 10ng of RNA was reverse transcribed using TaqMan MicroRNA Reverse Transcription Kit (Life Technologies #4366596) with RT primers specific for *miR-126* (*002228*) and control *snoRNA234 (0001234)*. Real Time PCR was performed using TaqMan Universal PCR Master Mix (Life Technologies #4324018) and TaqMan probes for *miR-126* and control s*noRNA234*.

RNA sequencing and analysis

RNA sequencing—Decidua-free placental tissue at E9.5 was isolated in cold PBS and flash frozen in liquid nitrogen. RNA was isolated using Trizol (Invitrogen). All RNA samples with RIN>7 were used for library preparation. Poly-A library preparation was performed using the TruSeq RNA Sample Preparation Kit (Illumina) at the Reproductive Genomics core facility (Cornell University) per standard protocols. The libraries were then sequenced using Illumina's HiSeq 2000 multiplexed in a single lane. Fastq files were generated with bcl2fastq 1.8.4 (Illumina) and will be deposited in the Gene Expression Omnibus (GEO) database.

RNA sequencing analysis—After ensuring high quality of the data, sequence reads for each library were mapped independently to the mouse genome assembly mm10, using the spliced aligner TopHat. For each library the number of sequence reads overlapping at any given nucleotide position in the reference genome was estimated at a 100-bp resolution. Mapped reads were quantified against the annotated mm10 transcriptome and the number of fragments originating from individual genes was estimated using the Cuffdiff program of the Cufflinks package. Count data was used to identify differential transcript expression and multiple hypotheses testing using DESeq2 package. The genes were filtered requiring at least 2 samples to have FPKM 2 and at least 2 (of 6) samples to have CPM (transcriptome-mapped reads) 5 for expression, and a trimmed-range (20th-80th percentile to avoid singleton-outlier genes) of 1.5-fold variation across samples. The PCA and hierarchical clustering analysis was performed using log2-transformed FPKM values for 3293 genes that were selected based on being expressed and variable among the samples.

DNA methylation analysis

Pyrosequencing—DNA was isolated from decidua-free placentas at E12.5 and submitted to EpigenDx for site-specific methylation analysis. DNA methylation analysis of the Igf2/H19 imprint control center was performed by EpigenDx (http://www.epigendx.com/).

Reduced Represented Bisulphite Sequencing (RRBS)—High quality genomic DNA was isolated from E12.5 decidua-free placentas (n=3) using standard phenol chloroform extraction and ethanol precipitation. RRBS was performed by the Epigenomics core at WCMC as follows: i) 5, 50 or 1000 ng of high quality genomic DNA were digested with 200 U of MspI (NEB R0106S) in a 100 ml reaction for up to 16 hours at 37°C. DNA was isolated using standard phenol chloroform extraction and ethanol precipitation and resuspended into 10 mM Tris pH 8.0.ii) End repair of digested DNA was performed using 15 U of T4 DNA polymerase (NEB M0203L), 5 U of Klenow DNA polymerase (NEB M0210L), 50 U of T4 Polynucleotide Kinase (NEB M0201L), 4 ml of premixed nucleotide triphosphates each at 10 mM (NEB N0447L) using T4 DNA ligase buffer with 10 mM dATP (NEB B0202S). The reaction was incubated at 20°C for 30 minutes and products were isolated using QIAquick PCR purification columns (Qiagen). iii) Adenylation was performed using 15 U Klenow fragments (NEB M0212L) and 10 ml of dATP at 1 mM concentration. The reaction was incubated at 37°C for 30 minutes and products were isolated using MinElute PCR purification columns (Qiagen). iv) Adenylated DNA fragments were ligated with pre-annealed 5-methylcytosine-containing Illumina adapters using 2000 U T4 DNA ligase (NEB M0202T) and 1.2 mM final concentration of methylated adapters at 16°C for 16 hours. Products were isolated using MinElute columns (Qiagen). v) Library fragments of 150–175 and 175–225 bp run on 1.5% low range ultra agarose gel were isolated using the Qiaquick Gel Extraction kit (Qiagen). vi) Bisulfite treatment was performed using the EZ DNA Methylation Kit (Zymo Research). vii) PCR amplification for each library was performed using FastStart Hifidelity DNA Polymerase (Roche) and PCR products were isolated using AMPure XP beads (Agencort). viii) All amplified libraries underwent quality control steps including using Qubit 1.0 fluorometer and a Quant-iT dsDNA HS Assay Kit for quantitation (Invitrogen) and bioanalyzer visualization (Agilent 2100 Bioanalyzer). Bioinformatics analysis was performed by the Epigenomic core at WCMC.

Results

Embryonic lethality of *miR-126*$^{-/-}$ embryos and late gestational intra-uterine growth restriction in a C57BL/6J background

Previous studies showed that *miR-126*$^{-/-}$ mice in a mixed genetic background display angiogenic defects, including leaky vessels, hemorrhaging, and partial embryonic lethality with incomplete penetrance (Kuhnert et al., 2008; Wang et al., 2008). To explore the function of *miR-126* in a congenic background, we backcrossed *miR-126*$^{+/-}$ mice (Wang et al., 2008) for ten generations into a C57BL/6J background. Intercrosses of congenic *miR-126*$^{+/-}$ mice failed to produce any surviving *miR-126*$^{-/-}$ pups at postnatal day10 (P10) (Fig. 1A). To determine the time of demise of *miR-126*$^{-/-}$ embryos, litters from *miR-126*$^{+/-}$ intercrosses were genotyped at different gestational stages. Only 6% (3 out of 52) of embryos at embryonic day 18.5 (E18.5) and 12% (14 out of 112) at E15.5 were *miR-126*$^{-/-}$. However, at E12.5, *miR-126*$^{-/-}$ embryos were observed at the expected 25% ratio (24 out of 98) (Fig. 1A). Vascular defects, including hemorrhaging at E12.5 and systemic edema at E15.5 (Kuhnert et al., 2008; Wang et al., 2008) were observed with complete penetrance in *miR-126*$^{-/-}$ embryos in a congenic C57BL/6J background (Fig. 1B). A fraction of

miR-126$^{+/-}$ embryos (~50%) displayed similar vascular defects. Analysis of E12.5 embryos derived from single heterozygous parents revealed that vascular hemorrhaging occurred only when the mutant *miR-126* allele was inherited from the father, suggesting an imprinting effect, and was observed in one-third of the heterozygous progeny (Supplemental Table S1). We next measured the sizes and weights of embryos and placentas at E12.5 and E15.5. *miR-126*$^{-/-}$ embryos at E15.5 had significantly lower crown-to-rump lengths and reduced wet weights when compared to *miR-126*$^{+/+}$ littermates (Fig. 1D), consistent with late gestational intra-uterine growth restriction (IUGR). No significant differences in weights and crown to rump lengths between *miR-126*$^{-/-}$ and *miR-126*$^{+/+}$ embryos were detected at E12.5 (Fig. 1C). Furthermore, no significant differences in placental lengths and weights were detected at E12.5 or E15.5 (Fig. 1C,D).

miR-126 is expressed by trophoblast and endothelial cells of the placenta.

During embryonic development, *Egfl7* and *miR-126* expression is restricted to the endothelium (Bambino et al., 2014; Fitch et al., 2004; Parker et al., 2004; Wang et al., 2008). Interestingly, during placental development *Egfl7* is expressed in the trophectoderm, in trophoblast stem cells (TSCs) and in junctional zone trophoblasts, in addition to maternal and fetal endothelial cells (Lacko et al., 2014).

To visualize localization of miR-126 in the murine placenta, we performed *in situ* hybridization using a *miR-126* specific locked nucleic acid (LNA) probe. *miR-126*$^{-/-}$ littermate placentas were used as controls for probe specificity. At E12.5, *miR-126* is expressed in the endothelial cells and in most trophoblast subtypes of the placenta (Fig. 2A(i)). Specifically, in the fetal labyrinth, we observed miR-126 transcripts in endothelial cells (Fig. 2A (iii), black arrows) and in syncytiotrophoblasts (Fig. 2A(iii), red arrows). miR-126 is also localized in the parietal trophoblast giant cells (Fig. 2A(v), red arrows) and in spongiotrophoblasts and glycogen trophoblasts (Fig. 2A(v), black arrows) of the junctional zone. No positive signal was detected in the labyrinth or junctional zones of *miR-126*$^{-/-}$ placentas demonstrating specificity of the probe (Fig. 2A(ii)(iv)(vi)). Similarly, we also detected *miR-126* expression in syncytiotrophoblasts (Fig. 2B, blue arrow), and in fetal endothelial cells (Fig. 2B, black arrow) in sections of term human placentas. No positive signal was detected in tissue hybridized with a scrambled LNA probe (Fig. 2B). Levels of *miR-126* expression were comparable in *miR-126*$^{+/+}$ E12.5 placentas and embryos, and undetectable in *miR-126*$^{-/-}$ embryos and placentas, as determined by quantitative RT-PCR (Fig. 2C). *miR-126* expression was at comparable levels in *miR-126*$^{+/+}$ trophoblast stem cells (TSCs) and embryonic stem cells (ESCs), and undetectable in *miR-126*$^{-/-}$ TSCs as determined by quantitative RT-PCR (Fig. 2D). *miR-126* is expressed in the placenta at E9.5, and its expression changes dynamically in the placenta throughout gestation (Fig. 2E). Together, these findings demonstrate that *miR-126* is expressed in TSC and the trophoblast lineage in murine and human placentas, in addition to its expression in fetal endothelial cells, similar to what we reported for its host gene, *Egfl7* (Lacko et al. 2014).

Hyperplasia of the junctional zone from increased numbers of glycogen trophoblasts in *miR-126⁻/⁻* placentas at E15.5

To investigate the phenotype of the *miR-126* loss-of function mutation in the placenta, we performed immunohistochemical analysis of the various placental compartments at E15.5, the developmental stage at which fetal growth restriction is apparent.

Unexpectedly, in contrast to the vascular defects observed in *miR-126⁻/⁻* embryos, including hemorrhaging, a reduced vascular plexus, and clusters of poorly differentiated endothelial cells (Fig. 1B, Supplemental Fig.S1), no gross morphological abnormalities were observed in the vasculature of the fetal labyrinth from *miR-126⁻/⁻* placentas (Fig. 3A and Supplemental Fig. S2). We measured average vessel area, numbers of proliferating endothelial cells and blood spaces in placentas at E12.5. There were no significant differences in average vessel area or fetal blood space (Fig. 3B, C) or numbers of proliferating endothelial cells (ERG⁺ EdU⁺) (Fig. 3D, E, F) in *miR-126⁻/⁻* placentas compared to *miR-126⁺/⁺* placentas.

Placental sections from E15.5 *miR-126⁻/⁻* (n=5) and *miR-126⁺/⁺* (n=6) littermates were immunostained with TPBPA antibodies to mark junctional zone (JZ) trophoblasts, and CD31 antibodies to mark endothelial cells of the fetal labyrinth (Lab) and the maternal decidua. Visual inspection showed an enlarged JZ in *miR-126⁻/⁻* placentas (Fig. 4A). Quantitative analysis showed a significant increase of the junctional zone area concomitant with a significant decrease in fetal labyrinth area in *miR-126⁻/⁻* placentas (Fig. 4B). The increase in junctional zone area is a result of significantly increased numbers of TPBPA⁺ trophoblast cells in *miR-126⁻/⁻* placentas compared to *miR-126⁺/⁺* littermates (Fig. 4C). No significant differences in the size of the decidua or of the total placental area between *miR-126⁺/⁺* and *miR-126⁻/⁻* placentas were detected (Fig. 4B and not shown). Placental labyrinth and junctional zone areas in *miR-126⁻/⁻* and *miR-126⁺/⁺* conceptuses were similar in size at E12.5 (Fig. 3G, H).

The observed expansion of the junctional zone in E15.5 *miR-126⁻/⁻* placentas suggested an increase in the numbers of spongiotrophoblasts (SpTs), glycogen trophoblasts (GlyTs), or both as the underlying cause. To identify the affected cell type(s), we performed co-immunostaining of E15.5 miR-126⁺/⁺ and miR-126⁻/⁻ placentas with antibodies for TPBPA and CDKN1C (Fig. 4D). Spongiotrophoblasts and glycogen trophoblasts of the junctional zone express the trophoblast specific gene *Tpbpa* (Adamson et al., 2002). Placental GlyTs but not SpTs express the imprinted gene *Cdkn1c* (Coan et al., 2006; Georgiades et al., 2002). Clusters of GlyTs (TPBPA⁺CDKN1C⁺) were detected in the junctional zones of *miR-126⁻/⁻* and *miR-126⁺/⁺* placentas (Fig. 4D, arrows). Quantification of GlyTs and SpTs showed that *miR-126⁻/⁻* placentas contain significantly increased numbers of TPBPA⁺CDKN1C⁺ GlyTs in the junctional zone (Fig. 4E). In contrast, no significant difference in the numbers of TPBPA⁺CDKN1C⁻ SpTs was detected (Fig. 4F). We also biochemically quantified the glycogen content in the placental tissue (Kemp and Van Heijningen, 1954). *miR-126⁻/⁻* placental tissue contained significantly increased amounts of glycogen when compared to *miR-126⁺/⁺* littermates (Fig. 4G). Together, these results indicate that *miR-126⁻/⁻* placentas contain increased numbers of glycogen trophoblasts that results in a significantly increased junctional zone area and reduced fetal labyrinth at E15.5. Our data are consistent with the

reduced labyrinth area as a cause for the observed IUGR and reduced viability of *miR-126*$^{-/-}$ embryos at E15.5, although the increased GlyT population and vascular defects in the embryos may contribute to this phenotype as well (Fig. 1A and 1D).

Increased numbers of proliferating glycogen trophoblast progenitors in *miR-126*$^{-/-}$ placentas at E13.5

To determine if the increased number of GlyTs in the junctional zone was a result of increased cell proliferation, we performed an EdU proliferation assay. EdU was intravenously injected into E15.5 pregnant females from *miR-126*$^{+/-}$ intercrosses, followed by co-immunostaining of placental sections with antibodies for CDKN1C and TPBPA. Few proliferating cells were detected in the junctional zone of E15.5 *mir-126*$^{+/+}$ and *miR-126*$^{-/-}$ placentas (Fig. S3). This is consistent with a previous study reporting a 4-fold increase in spongiotrophoblasts and a 250-fold increase in glycogen trophoblasts between E12.5 and E16.5, with proliferation ceasing by E16.5 (Coan et al., 2006). To quantify proliferating progenitor cells at the time of trophoblast cell proliferation in the junctional zone, we repeated EdU injections and immunostaining of placentas at E13.5 (Fig. 5A). Quantification of glycogen trophoblast progenitors and proliferating glycogen trophoblast progenitors in the junctional zone revealed that *miR-126*$^{-/-}$ placentas (n=4) contain a significantly higher fraction of CDKN1C$^+$TPBPA$^+$ glycogen trophoblast progenitors (Fig. 5B) and, most importantly, a significantly higher proportion of EdU$^+$CDKN1C$^+$TPBPA$^+$ proliferating glycogen trophoblast progenitors (Fig. 5C) when compared to *miR-126*$^{+/+}$ placentas (n=4). No significant differences in the fraction of TPBPA$^+$CDKN1C$^-$ spongiotrophoblast progenitors (Fig. 5D) or EdU$^+$TPBPA$^+$ proliferating trophoblast progenitors were detected in the junctional zone between *miR-126*$^{+/+}$ and *miR-126*$^{-/-}$ placentas (Fig. 5E). These results indicate that loss-of *miR-126* function leads to increased numbers of proliferating glycogen trophoblast progenitors at E13.5, resulting in increased numbers of differentiated GlyTs and an expanded junctional zone in E15.5 placentas.

Transcriptome profiling on E9.5 *miR-126*$^{-/-}$ placentas

To identify differentially expressed genes in *miR-126*$^{-/-}$ versus *miR-126*$^{+/+}$ placental trophoblasts, we performed transcriptome profiling by RNA sequencing on E9.5 placentas containing the junctional zone and the labyrinth layers. At this stage, the placenta can be easily separated from the maternal decidua and the allantois. It contains primarily trophoblast progenitors and early differentiated trophoblasts that participate in the formation of the labyrinth and junctional zone, as well as extraembryonic mesoderm, thus facilitating the investigation of the transcriptome regulated by *miR-126* prior to the onset blood flow in the fetal labyrinth.

Gene expression profiling revealed 177 significantly upregulated and 48 significantly downregulated genes with a fold change 1.5 in a log2 scale in *miR-126*$^{-/-}$ placentas compared to *miR-126*$^{+/+}$ placentas at E9.5 (Fig. 6A). Genes dysregulated in *miR-126*$^{-/-}$ placentas are listed in Supplemental Tables S2 and S3. Importantly, a large number of GlyT- and trophoblast-specific genes, and genes with known roles in placental development, glucose and fat metabolism, retinoic acid (RA) pathway, and angiogenesis are dysregulated in E9.5 *miR-126*$^{-/-}$ placentas (Fig. 6B and Supplemental Table S4).

Placental trophoblasts specifically express a set of prolactin genes that encode metabolic pregnancy hormones (Simmons et al., 2008). Interestingly, E9.5 *miR-126⁻/⁻* placentas display significant upregulation of the GlyT specific prolactin genes *Prl6a1*, *Prl7b1*, *Prl7c1*, retinaldehyde dehydrogenase 3 (*Raldh3*), *Aldh1a3*, and the protocadherin gene *Pcdh12* when compared to *miR-126⁺/⁺* placentas (Fig 6B). Significantly increased expression of several GlyT specific genes (*Prl6a1*, *Prl7c1*, *Pcdh12*) was validated by qRT-PCR (Fig 6C). The upstream regulatory regions of GlyT specific prolactin genes contain modules of transcription factor binding sites that have been proposed to regulate cell-type specific expression in the placenta, including GFI1, GATA3, PRRX2, AP1, NKX3A (Simmons et al., 2008). Several of these transcription factors or closely related family members of these transcription factors (*Gfi1*, *Prrx1*, *Gata1*) are also significantly upregulated in *miR-126⁻/⁻* placentas (Fig. 6B). In addition, expression levels of several placenta-specific genes, including *Tpbpa*, *Tpbpb*, *Hbb-y*, *Hba-x*, *Amn*, *Ceacam3*, *Pappa2* and the cathepsin genes *Cts7* and *Cts8*, were significantly increased in *miR-126⁻/⁻* placentas (Fig. 6B, Supplemental Table S4).

miR-126⁻/⁻ placentas also displayed significant upregulation of several genes involved in glucose metabolism (*Igfbp1*, *Igfbp2*, *Asb4*, *Plagl1*, *Aplnr*, *Glut3/Slc2a3*) and fat metabolism (*Fabp1*, *Fabp3*). Additionally, expression of several retinoic acid pathway-related genes (*Ttr*, *Rbp4*, *Aldh1a3*) and genes controlling angiogenesis (*Vcam1*, *Itga4*, *Flt1*, *Angpt1*, *Nrp1*, *Itga3*) were upregulated in *miR-126⁻/⁻* placentas (Fig. 6B, Supplemental Table S4). Pathway analysis (IPA, Qiagen) on differentially expressed genes revealed an enrichment of genes in several pathways including LXR/RXR activation pathway, acute phase response signaling, FAK signaling and VEGF signaling (Fig. 6D). Positive z-score for LXR/RXR pathway indicates a significantly increased overall activation of the retinoic acid pathway in *miR-126⁻/⁻* placentas. GlyT cells in the placenta have been suggested to act as a source of retinoic acid, which can act in an autocrine manner to facilitate proliferation, differentiation and migration of these cells (Outhwaite et al., 2015).

Dysregulated genes were also categorized based on Gene Ontology (Supplemental Fig. S4). Gene ontology analysis of the significantly dysregulated genes uncovered broad molecular and cellular functions, and physiological system development and function categories (Supplemental Fig. S4).

miR-126 affects imprinted gene expression in the placenta and regulates DNA methylation

Several known regulators of junctional zone trophoblast development at later developmental stages are imprinted genes (Cleaton et al., 2014; Ferguson-Smith et al., 2001; Lefebvre, 2012). Located on the distal end of chromosome 7, the *Igf2/H19* cluster contains the imprinted genes *Igf2* and *H19*. Allele specific expression is regulated by DNA methylation at an imprint control center located 2kb upstream of H19 (Trembley and Thorvaldsen). Bi-allelic expression of *Igf2*, via deletion of the imprint control center results in an increase in the number of GlyTs and glycogen content in the placenta (Esquiliano et al., 2009).

For expression analysis, we separated the fetal part of the placenta from the maternal decidua at E12.5 to eliminate contamination from the maternal tissue. We analyzed expression levels of the imprinted genes located in the *Igf2/H19* cluster located on the distal

end of chromosome 7 (Fig. 7A) by qRT-PCR, and DNA methylation at the imprint control center by Pyrosequencing in E12.5 placentas. *miR-126⁻/⁻* placentas show significantly reduced expression of *Igf2* and significantly elevated *H19* expression when compared to *miR-126⁺/⁺* placentas (Fig. 7B). In contrast, *Igf2* and *H19* expression is unchanged between E12.5 *miR-126⁻/⁻* and *miR-126⁺/⁺* embryos (Supplemental Fig. S5A). We analyzed DNA methylation of CpG dinucleotides at the imprint control center, which contains four binding sites for the repressor CTCF (Bell and Felsenfeld, 2000; Hark et al., 2000; Kanduri et al., 2000). Whereas *miR-126⁻/⁻* placentas displayed no significant differences in DNA methylation at the first two CTCF binding sites, CTCF1 and CTCF2 (Fig. 7C(i)(ii)), several CpGs were significantly hypermethylated in CTCF3 and CTCF4 binding sites as compared to *miR-126⁺/⁺* placentas (Fig. 7C (iii)(iv)).

The *Kcnq1ot1* cluster on chromosome 7 contains several imprinted genes with important roles in placental junctional zone development (Fig. 7D). Loss of *Cdkn1c* leads to GlyT differentiation defects (Tunster et al., 2011). Loss and gain of function of *Phlda2* results in abnormal SpT development and glycogen storage in the placenta (Tunster et al., 2010). *Ascl2* hypomorphs have reduced cell numbers of SpTs and no GlyTs (Oh-McGinnis et al., 2011). Expression of imprinted genes in this cluster is controlled by transcription of the long non-coding RNA Kcnq1ot1 (Lewis et al., 2004). The imprint control center for this cluster, KvDMR1, is located at the *Kcnq1ot1* promoter. DNA methylation of KvDMR1 on the maternal allele suppresses transcription of *Kcnq1ot1* ensuring allele specific expression of Kcnq1ot1 and other imprinted genes in this cluster (Kanduri et al., 2002).

We analyzed expression levels of the imprinted genes located in the *Kcnq1ot1* cluster by qRT-PCR, and DNA methylation at KvDMR1 by Reduced Representation Bisulphite Sequencing (RRBS) in E12.5 placentas. *miR-126⁻/⁻* placentas display significantly reduced expression of *Kcnq1ot1* and no significant difference in *Kcnq1* expression (Fig. 7E). Expression levels of *Cdkn1c* were significantly reduced, whereas *Phlda2* expression levels were elevated in *miR-126⁻/⁻* placentas without reaching significance when compared to *miR-126⁺/⁺* placentas (Fig. 7E). In contrast, expression of these imprinted genes is unchanged in E12.5 *miR-126⁻/⁻* embryos (Supplemental Fig. S5B). At KvDMR1, *miR-126⁻/⁻* placentas display significantly elevated DNA methylation at several CpGs when compared to *miR-126⁺/⁺* placentas (Fig. 7F).

To investigate if defects in DNA methylation were restricted to the clusters on the distal end of chromosome 7, we analyzed expression levels of the imprinted genes located at other genomic locations and DNA methylation at their ICRs (Fig. 7G). *Grb10* is a maternally expressed gene on chromosome 11, and its ICR is methylated on the maternally inherited chromosome. Its deletion leads to placental defects and overgrowth of the embryo and placenta (Charalambous et al., 2010). *Peg3* is a paternally expressed gene located in the centromeric region of chromosome 7 that regulates transcription of several placental-specific gene families (Kim et al., 2013); its ICR is methylated on the maternally inherited chromosome. Expression levels of both *Grb10* and *Peg3* are significantly downregulated in *miR-126⁻/⁻* placentas at E12.5 (Fig. 7H). At the *Grb10* ICR, several CpGs display significantly elevated methylation in *miR-126⁻/⁻* placentas when compared to *miR-126⁺/⁺* placentas (Fig. 7I). At the *Peg3* ICR, there were no significant differences in DNA

methylation in E12.5 placentas (Fig. 7J). miR-$126^{-/-}$ embryos do not display any significant differences in expression of $Grb10$ and $Peg3$ (Supplemental Fig. S5C).

We also analyzed genome-wide differences in DNA methylation at CpG rich regions in E12.5 placentas by RRBS. miR-$126^{-/-}$ placentas display significant hypermethylation at a genome-wide level when compared to miR-$126^{+/+}$ placentas. Specifically, the percentage of differentially methylated regions per chromosome, with a methylation difference of >20% and a q value of <0.01, was increased by ~1.5% in miR-$126^{-/-}$ placentas (Fig. 7K). Together, these results indicate that loss of miR-126 function results in genome wide hypermethylation, including imprint control centers of multiple imprinted gene clusters, and in aberrant expression of imprinted genes in the placenta.

Discussion

The results presented in this study reveal a novel role for miR-126 in regulating GlyT proliferation, DNA methylation and imprinted gene expression during placental development. Loss-of miR-126 function resulted in a mutant phenotype that was restricted to the trophoblasts of the placenta. miR-$126^{-/-}$ placentas contain increased numbers of proliferating GlyT progenitors resulting in hyperplasia of the junctional zone at the expense of the fetal labyrinth, concomitant with late gestational IUGR of the embryos. This phenotype was unexpected, since miR-126 expression was thought to be endothelial cell-specific, and miR-$126^{-/-}$ embryos and adult mice display vascular phenotypes and defects in angiogenesis (Kuhnert et al., 2008; Wang et al., 2008). In contrast, overt vascular phenotypes were absent in the fetal labyrinth of miR-$126^{-/-}$ placentas (Fig. 3 and Supplemental Fig. S2). This result may reflect the fact that the endothelial cell lineage in the fetal labyrinth is derived from the extraembryonic mesoderm of the allantois, whereas all embryonic and adult endothelial cells are derived from the mesoderm of the embryo proper. In support, the transcriptome of the placental endothelium is unique when compared to that of other vascular beds (Nolan et al., 2013). Intriguingly, mice with loss-of-function of the host gene $Egfl7$ display vascular patterning defects in the fetal labyrinth but lack an overt phenotype in the embryonic or adult vasculature (Lacko et al., 2017).

The integration of microRNAs into introns of protein coding genes provides a common mechanism to coordinate the expression and the regulatory functions of microRNAs with the gene networks regulated by the host gene (Liu and Olson, 2010; Wang et al., 2008). Co-expression of miR-126 and $Egfl7$ in the endothelium of embryos and adult mice is controlled by an upstream 5.4-kb regulatory region that contains conserved consensus sequences for binding of ETS transcription factors (Bambino et al., 2014; Wang et al., 2008). miR-126 is generated from a retained intron in a subset of Egfl7 pre-mRNAs (Wang et al., 2008). In the placenta, in addition to their expression in the fetal and maternal endothelium, miR-126 and $Egfl7$ are co-expressed in the trophoblast lineage. Specifically, we detected miR-126 transcripts, and Egfl7 transcripts and protein in junctional zone trophoblasts of the murine placenta and in cytotrophoblasts and syncytiotrophoblasts of term human placenta, and in mouse TSCs (Lacko et al., 2014). Interestingly, miR-126 was also detected in immune cells at the maternal-fetal interphase of the decidua (punctate staining in Fig. 2A (i) and (ii)).

Our study is the first to implicate a role for a microRNA in GlyT proliferation and regulation of imprinted gene expression specifically in the placenta. The function of the GlyT lineage in the placenta is incompletely understood; however, their migration into the decidua during late gestation and subsequent release of glucose into the maternal bloodstream supports the hypothesis that they are important for supplementing maternal nutrient resources and for regulating embryonic growth during late gestation (Coan et al., 2006).

Although some data suggests the existence of distinct GlyT progenitor during early placental development, nothing is known about regulators of early GlyT development in the placenta. One study characterized GlyT specific prolactin gene signatures in placentas between E7.5 and E18.5, demonstrating that several prolactin family members, including *Prl6a1, Prl7b1, Prl7c1* are already expressed at E8.5 in the ectoplacental cone and become later restricted to GlyT cells (Simmons et al., 2008). This study also identified transcription factor binding modules that potentially regulate GlyT specific expression. However, it is unknown if these prolactin genes or the transcription factors can drive GlyT development and proliferation during placental development. Interestingly, we found that *miR-126*$^{-/-}$ placentas at E9.5 significantly overexpress GlyT specific prolactin genes (*Prl6a1, Prl7b1, Prl7c1*) and also several transcription factors or their closely related family members proposed to bind to their promoters (*Gfi1, Gata1, Prrx1*). It is possible that *miR-126* dependent upregulation of these transcription factors and/or the prolactin genes drives GlyT progenitor differentiation during early development and GlyT proliferation during mid gestation.

The parental conflict theory proposes that imprinted genes embody regulation of placental endocrine function during pregnancy, and that genomic imprinting evolved to regulate energy exchange between the mother and the fetus (Cleaton et al., 2014; Hudson et al., 2010; John, 2017; Lefebvre, 2012). The distal portion of mouse chromosome 7 contains several imprinted genes (*Igf2, H19, Kcnq1ot1, Cdkn1c, Phlda2, Ascl2*) that are organized into two distinct and independently regulated clusters. Mice with gain- and loss-of function mutations, as well as mutants with bi-allelic gene expression, display defects in glycogen cell proliferation and differentiation (Constancia et al., 2002; Esquiliano et al., 2009; Oh-McGinnis et al., 2011; Salas et al., 2004; Sferruzzi-Perri et al., 2011; Tunster et al., 2010; Tunster et al., 2011). Importantly, these defects are similar to the phenotypes observed in *miR-126*$^{-/-}$ placentas. Furthermore, *miR-126*$^{-/-}$ placentas display dysregulated expression of *Igf2, H19*, *Kcnq1ot1*, *Cdkn1c* and *Phlda2* at E12.5. We reason that the glycogen trophoblast phenotype we observed in *miR-126*$^{-/-}$ placentas does not reflect effects seen from dysregulated expression of a single imprinted gene or gene cluster, but potentially arises from small gene expression changes of several imprinted and non-imprinted genes resulting from a global defect in maintenance DNA methylation in rapidly dividing cells. Expression changes detected in some imprinted genes in *miR-126*$^{-/-}$ placentas are opposite to what would be predicted from changes in DNA methylation at their ICRs. We reason that *miR-126* mediated changes in DNA methylation at regions outside the ICRs, as well as accessibility of enhancer element regions to chromatin changes and transcription factor binding are affecting expression of the imprinted genes.

Sporadic hypermethylation in *miR-126*$^{-/-}$ placentas is not restricted to the imprint control centers but is pervasive throughout the genome. Our analysis of methylation of CpGs-rich

regions in the placental genome demonstrates that loss of *miR-126* results in significant hypermethylation of 20% in 1–3% of CpG dinucleotides in all the chromosomes (Fig. 7K). However, the inbred background of the mutant mice precludes allele specific analysis. Investigating the potential loss of imprinting in the placenta resulting from the deletion of *miR-126* would require extensive allele specific expression and methylation analysis on placentas from *miR-126*$^{+/-}$ (*M. mus. domesticus*) × *miR-126*$^{+/-}$ (*M. mus. castaneus*) intercrosses, which is beyond the scope of the present study.

The changes in global DNA methylation indicate that *miR-126* may regulate, either directly or indirectly, one or several major regulators of DNA methylation in the placenta. However, changes in expression were relatively small for *Dnmt3a* and *Tet1* and varied in a dynamic temporal fashion for *Dnmt1* (data not shown). Moreover, none of the DNA methyl transferases or *Tet* genes possesses canonical binding sites for *miR-126* in their 3'UTRs, suggesting that their expression is not directly regulated by *miR-126*. Furthermore, none of the known regulators of *Dnmt1* are direct targets of *miR-126* and they do not possess canonical binding sites in their 3'UTRs. miRNAs are known to regulate several genes in a single pathway to affect a signaling outcome. It is conceivable that *miR-126* regulates DNA methylation in the placenta by inhibiting translation of several known and novel regulators of DNA methylation in the placenta.

Mutant phenotypes in mice with gain- or loss-of *miRNA* function are mostly subtle and result in few overt developmental abnormalities (Park et al., 2012; Vidigal and Ventura, 2015). It is striking that a loss-of *miR-126* function resulted in complete embryonic lethality, vascular phenotypes in the embryos, defects in glycogen cell proliferation in the placenta and IUGR. In fact, to our knowledge this is the first miRNA mutant for which this prominent developmental phenotype has been reported. Recently, defects in placental growth and development have been reported for targeted deletions of the microRNA miR-675 that is embedded with the *H19* gene, the miR-290 cluster, and a large microRNA cluster embedded in the *Sfmbt2* gene (Inoue et al., 2017; Keniry et al., 2012; Paikari et al., 2017). Our study also establishes the importance of the genetic background for the phenotypes detected in *miR-126* mutant mice. In a mixed genetic background, post-natal lethality and embryonic angiogenesis defects were incompletely penetrant (Kuhnert et al., 2008; Wang et al., 2008). In contrast, in an inbred C57BL/6J background, lethality at birth and embryonic angiogenesis defects were completely penetrant. Moreover, we also observed haploinsufficiency for *miR-126* with increased lethality of *miR-126*$^{+/-}$ pups at birth.

Statistics

Data are represented as mean ± SEM. The data were analyzed using a student's t-test. Statistical significance was defined as *P<0.05, **P<0.01, ***P<0.001, unless otherwise noted.

Supplementary Material

Refer to Web version on PubMed Central for supplementary material.
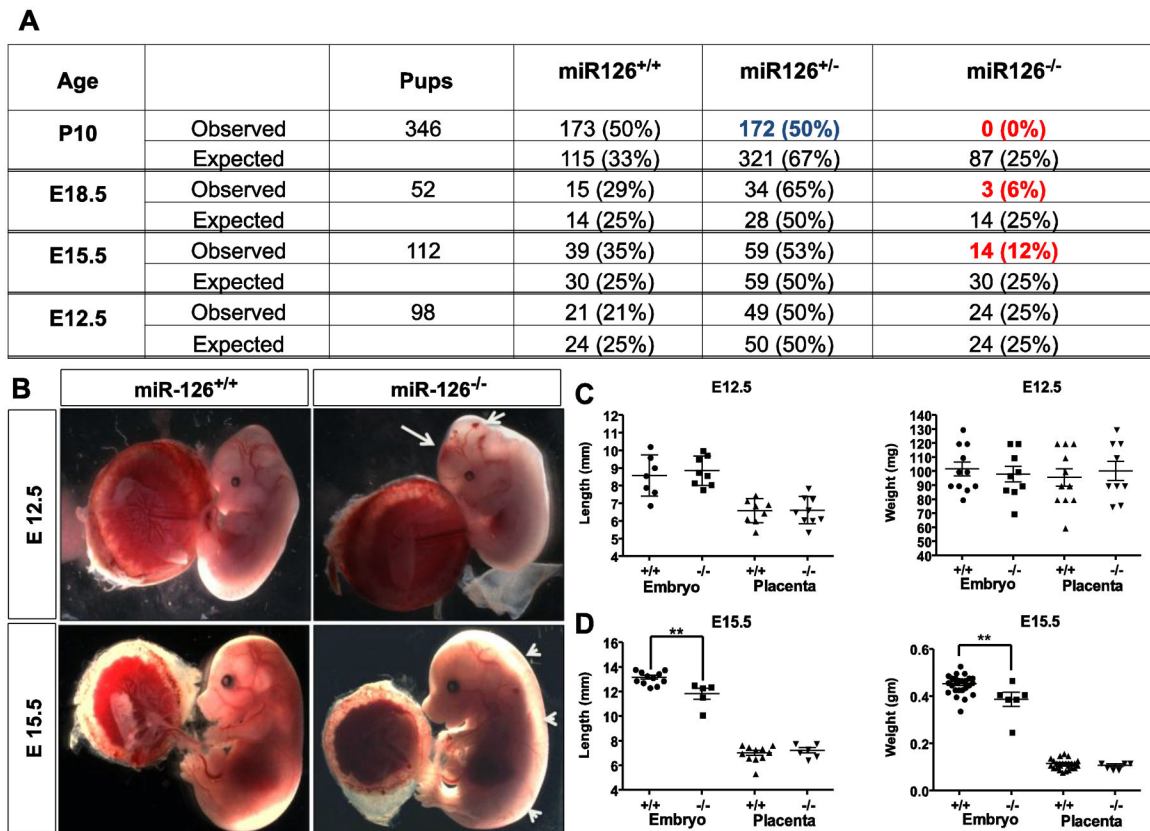
Acknowledgments

References

Adamson SL, Lu Y, Whiteley KJ, Holmyard D, Hemberger M, Pfarrer C and Cross JC (2002). Interactions between trophoblast cells and the maternal and fetal circulation in the mouse placenta. Dev Biol 250, 358–373. [PubMed: 12376109]

Bambino K, Lacko LA, Hajjar KA and Stuhlmann H (2014). Epidermal growth factor-like domain 7 is a marker of the endothelial lineage and active angiogenesis. Genesis 52, 657–670. [PubMed: 24740971]

Barlow DP and Bartolomei MS (2014). Genomic imprinting in mammals. Cold Spring Harb Perspect Biol 6.

Bell AC and Felsenfeld G (2000). Methylation of a CTCF-dependent boundary controls imprinted expression of the Igf2 gene. Nature 405, 482–485. [PubMed: 10839546]

Charalambous M, Cowley M, Geoghegan F, Smith FM, Radford EJ, Marlow BP, Graham CF, Hurst LD and Ward A (2010). Maternally-inherited Grb10 reduces placental size and efficiency. Dev Biol 337, 1–8. [PubMed: 19833122]

Chhabra A, Lechner AJ, Ueno M, Acharya A, Van Handel B, Wang Y, Iruela-Arispe ML, Tallquist MD and Mikkola HK (2012). Trophoblasts regulate the placental hematopoietic niche through PDGF-B signaling. Dev Cell 22, 651–659. [PubMed: 22387002]

Cleaton MA, Edwards CA and Ferguson-Smith AC (2014). Phenotypic outcomes of imprinted gene models in mice: elucidation of pre- and postnatal functions of imprinted genes. Annu Rev Genomics Hum Genet 15, 93–126. [PubMed: 24898037]

Coan PM, Conroy N, Burton GJ and Ferguson-Smith AC (2006). Origin and characteristics of glycogen cells in the developing murine placenta. Dev Dyn 235, 3280–3294. [PubMed: 17039549]

Constancia M, Hemberger M, Hughes J, Dean W, Ferguson-Smith A, Fundele R, Stewart F, Kelsey G, Fowden A, Sibley C, et al. (2002). Placental-specific IGF-II is a major modulator of placental and fetal growth. Nature 417, 945–948. [PubMed: 12087403]

Esquiliano DR, Guo W, Liang L, Dikkes P and Lopez MF (2009). Placental glycogen stores are increased in mice with H19 null mutations but not in those with insulin or IGF type 1 receptor mutations. Placenta 30, 693–699. [PubMed: 19524295]

Ferguson-Smith AC, Tevendale M, Georgiades P and Grandjean V (2001). Balanced translocations for the analysis of imprinted regions of the mouse genome. Methods Mol Biol 181, 41–54. [PubMed: 12843440]

Fish JE, Santoro MM, Morton SU, Yu S, Yeh RF, Wythe JD, Ivey KN, Bruneau BG, Stainier DY and Srivastava D (2008). miR-126 regulates angiogenic signaling and vascular integrity. Dev Cell 15, 272–284. [PubMed: 18694566]

Fitch MJ, Campagnolo L, Kuhnert F and Stuhlmann H (2004). Egfl7, a novel epidermal growth factor-domain gene expressed in endothelial cells. Dev Dyn 230, 316–324. [PubMed: 15162510]

Georgiades P, Ferguson-Smith AC and Burton GJ (2002). Comparative developmental anatomy of the murine and human definitive placentae. Placenta 23, 3–19. [PubMed: 11869088]

Georgiades P, Watkins M, Burton GJ and Ferguson-Smith AC (2001). Roles for genomic imprinting and the zygotic genome in placental development. Proc Natl Acad Sci U S A 98, 4522–4527. [PubMed: 11274372]

Gicquel C, Rossignol S, Cabrol S, Houang M, Steunou V, Barbu V, Danton F, Thibaud N, Le Merrer M, Burglen L, et al. (2005). Epimutation of the telomeric imprinting center region on chromosome 11p15 in Silver-Russell syndrome. Nat Genet 37, 1003–1007. [PubMed: 16086014]

Green BB, Kappil M, Lambertini L, Armstrong DA, Guerin DJ, Sharp AJ, Lester BM, Chen J and Marsit CJ (2015). Expression of imprinted genes in placenta is associated with infant neurobehavioral development. Epigenetics 10, 834–841. [PubMed: 26198301]

Hark AT, Schoenherr CJ, Katz DJ, Ingram RS, Levorse JM and Tilghman SM (2000). CTCF mediates methylation-sensitive enhancer-blocking activity at the H19/Igf2 locus. Nature 405, 486–489. [PubMed: 10839547]

Hudson QJ, Kulinski TM, Huetter SP and Barlow DP (2010). Genomic imprinting mechanisms in embryonic and extraembryonic mouse tissues. Heredity (Edinb) 105, 45–56. [PubMed: 20234385]

Inoue K, Hirose M, Inoue H, Hatanaka Y, Honda A, Hasegawa A, Mochida K and Ogura A (2017). The Rodent-Specific MicroRNA Cluster within the Sfmbt2 Gene Is Imprinted and Essential for Placental Development. Cell Rep 19, 949–956. [PubMed: 28467908]

John RM (2017). Imprinted genes and the regulation of placental endocrine function: Pregnancy and beyond. Placenta.

Kanduri C, Fitzpatrick G, Mukhopadhyay R, Kanduri M, Lobanenkov V, Higgins M and Ohlsson R (2002). A differentially methylated imprinting control region within the Kcnq1 locus harbors a methylation-sensitive chromatin insulator. J Biol Chem 277, 18106–18110. [PubMed: 11877438]

Kanduri C, Pant V, Loukinov D, Pugacheva E, Qi CF, Wolffe A, Ohlsson R and Lobanenkov VV (2000). Functional association of CTCF with the insulator upstream of the H19 gene is parent of origin-specific and methylation-sensitive. Curr Biol 10, 853–856. [PubMed: 10899010]

Kemp A and Van Heijningen AJ (1954). A colorimetric micro-method for the determination of glycogen in tissues. Biochem J 56, 646–648. [PubMed: 13159896]

Keniry A, Oxley D, Monnier P, Kyba M, Dandolo L, Smits G and Reik W (2012). The H19 lincRNA is a developmental reservoir of miR-675 that suppresses growth and Igf1r. Nat Cell Biol 14, 659–665. [PubMed: 22684254]

Kim J, Frey WD, He H, Kim H, Ekram MB, Bakshi A, Faisal M, Perera BP, Ye A and Teruyama R (2013). Peg3 mutational effects on reproduction and placenta-specific gene families. PLoS One 8, e83359. [PubMed: 24391757]

Kuhnert F, Mancuso MR, Hampton J, Stankunas K, Asano T, Chen CZ and Kuo CJ (2008). Attribution of vascular phenotypes of the murine Egfl7 locus to the microRNA miR-126. Development 135, 3989–3993. [PubMed: 18987025]

Lacko LA, Hurtado R, Hinds S, Poulos MG, Butler JM and Stuhlmann H (2017). Altered feto-placental vascularization, feto-placental malperfusion, and fetal growth restriction in mice with Egfl7 loss-of-function. Development.

Lacko LA, Massimiani M, Sones JL, Hurtado R, Salvi S, Ferrazzani S, Davisson RL, Campagnolo L and Stuhlmann H (2014). Novel expression of EGFL7 in placental trophoblast and endothelial cells and its implication in preeclampsia. Mech Dev 133, 163–176. [PubMed: 24751645]

Lefebvre L (2012). The placental imprintome and imprinted gene function in the trophoblast glycogen cell lineage. Reprod Biomed Online 25, 44–57. [PubMed: 22560119]

Lewis A, Mitsuya K, Umlauf D, Smith P, Dean W, Walter J, Higgins M, Feil R and Reik W (2004). Imprinting on distal chromosome 7 in the placenta involves repressive histone methylation independent of DNA methylation. Nat Genet 36, 1291–1295. [PubMed: 15516931]

Liu N and Olson EN (2010). MicroRNA regulatory networks in cardiovascular development. Dev Cell 18, 510–525. [PubMed: 20412767]

Lopez MF, Dikkes P, Zurakowski D and Villa-Komaroff L (1996). Insulin-like growth factor II affects the appearance and glycogen content of glycogen cells in the murine placenta. Endocrinology 137, 2100–2108. [PubMed: 8612553]

Maher ER and Reik W (2000). Beckwith-Wiedemann syndrome: imprinting in clusters revisited. J Clin Invest 105, 247–252. [PubMed: 10675349]

Maltepe E, Bakardjiev AI and Fisher SJ (2010). The placenta: transcriptional, epigenetic, and physiological integration during development. J Clin Invest 120, 1016–1025. [PubMed: 20364099]

Nielsen BS (2012). MicroRNA in situ hybridization. Methods Mol Biol 822, 67–84. [PubMed: 22144192]

Nolan DJ, Ginsberg M, Israely E, Palikuqi B, Poulos MG, James D, Ding BS, Schachterle W, Liu Y, Rosenwaks Z, et al. (2013). Molecular signatures of tissue-specific microvascular endothelial cell heterogeneity in organ maintenance and regeneration. Dev Cell 26, 204–219. [PubMed: 23871589]

Oh-McGinnis R, Bogutz AB and Lefebvre L (2011). Partial loss of Ascl2 function affects all three layers of the mature placenta and causes intrauterine growth restriction. Dev Biol 351, 277–286. [PubMed: 21238448]

Outhwaite JE, Natale BV, Natale DR and Simmons DG (2015). Expression of aldehyde dehydrogenase family 1, member A3 in glycogen trophoblast cells of the murine placenta. Placenta 36, 304–311. [PubMed: 25577283]

Paikari A, D. B. C, Saw D and Blelloch R (2017). The eutheria-specific miR-290 cluster modulates placental growth and maternal-fetal transport. Development 144, 3731–3743. [PubMed: 28935707]

Park CY, Jeker LT, Carver-Moore K, Oh A, Liu HJ, Cameron R, Richards H, Li Z, Adler D, Yoshinaga Y, et al. (2012). A resource for the conditional ablation of microRNAs in the mouse. Cell Rep 1, 385–391. [PubMed: 22570807]

Parker LH, Schmidt M, Jin SW, Gray AM, Beis D, Pham T, Frantz G, Palmieri S, Hillan K, Stainier DY, et al. (2004). The endothelial-cell-derived secreted factor Egfl7 regulates vascular tube formation. Nature 428, 754–758. [PubMed: 15085134]

Plasschaert RN and Bartolomei MS (2014). Genomic imprinting in development, growth, behavior and stem cells. Development 141, 1805–1813. [PubMed: 24757003]

Rossant J and Cross JC (2001). Placental development: lessons from mouse mutants. Nat Rev Genet 2, 538–548. [PubMed: 11433360]

Salas M, John R, Saxena A, Barton S, Frank D, Fitzpatrick G, Higgins MJ and Tycko B (2004). Placental growth retardation due to loss of imprinting of Phlda2. Mech Dev 121, 1199–1210. [PubMed: 15327781]

Schonherr N, Meyer E, Roos A, Schmidt A, Wollmann HA and Eggermann T (2007). The centromeric 11p15 imprinting centre is also involved in Silver-Russell syndrome. J Med Genet 44, 59–63. [PubMed: 16963484]

Sferruzzi-Perri AN, Vaughan OR, Coan PM, Suciu MC, Darbyshire R, Constancia M, Burton GJ and Fowden AL (2011). Placental-specific Igf2 deficiency alters developmental adaptations to undernutrition in mice. Endocrinology 152, 3202–3212. [PubMed: 21673101]

Simmons DG, Rawn S, Davies A, Hughes M and Cross JC (2008). Spatial and temporal expression of the 23 murine Prolactin/Placental Lactogen-related genes is not associated with their position in the locus. BMC Genomics 9, 352. [PubMed: 18662396]

Tanaka S, Kunath T, Hadjantonakis AK, Nagy A and Rossant J (1998). Promotion of trophoblast stem cell proliferation by FGF4. Science 282, 2072–2075. [PubMed: 9851926]

Tunster SJ, Jensen AB and John RM (2013). Imprinted genes in mouse placental development and the regulation of fetal energy stores. Reproduction 145, R117–137. [PubMed: 23445556]

Tunster SJ, Tycko B and John RM (2010). The imprinted Phlda2 gene regulates extraembryonic energy stores. Mol Cell Biol 30, 295–306. [PubMed: 19884348]

Tunster SJ, Van de Pette M and John RM (2011). Fetal overgrowth in the Cdkn1c mouse model of Beckwith-Wiedemann syndrome. Dis Model Mech 4, 814–821. [PubMed: 21729874]

Vidigal JA and Ventura A (2015). The biological functions of miRNAs: lessons from in vivo studies. Trends Cell Biol 25, 137–147. [PubMed: 25484347]

Wang S, Aurora AB, Johnson BA, Qi X, McAnally J, Hill JA, Richardson JA, Bassel-Duby R and Olson EN (2008). The endothelial-specific microRNA miR-126 governs vascular integrity and angiogenesis. Dev Cell 15, 261–271. [PubMed: 18694565]

Watson ED and Cross JC (2005). Development of structures and transport functions in the mouse placenta. Physiology (Bethesda) 20, 180–193. [PubMed: 15888575]

Highlights

- Placental expression of the microRNA *miR-126* is detected in trophoblast cells and endothelial cells

- *miR-126* plays a critical role in placental development affecting extra-embryonic energy stores

- Loss-of *miR-126* function results in increased glycogen trophoblast numbers, hyperplasia of the junctional zone and reduced fetal labyrinth

- Loss-of *miR-126* function leads to aberrant expression of imprinted genes and to DNA hypermethylation in the placenta.

A

Age		Pups	miR126⁺/⁺	miR126⁺/⁻	miR126⁻/⁻
P10	Observed	346	173 (50%)	**172 (50%)**	**0 (0%)**
	Expected		115 (33%)	321 (67%)	87 (25%)
E18.5	Observed	52	15 (29%)	34 (65%)	**3 (6%)**
	Expected		14 (25%)	28 (50%)	14 (25%)
E15.5	Observed	112	39 (35%)	59 (53%)	**14 (12%)**
	Expected		30 (25%)	59 (50%)	30 (25%)
E12.5	Observed	98	21 (21%)	49 (50%)	24 (25%)
	Expected		24 (25%)	50 (50%)	24 (25%)

Figure 1: *miR-126⁻/⁻* **mice in a congenic C57BL/6J background die in utero and display late gestational IUGR**

(A) Genotypes of offspring from *miR-126⁺/⁻* intercrosses. The observed and expected numbers of mice and embryos for each genotype at each developmental stage are shown. Loss of *miR-126⁻/⁻* embryos starts at E15.5, and lethality is fully penetrant at birth (highlighted in red). Recovery of heterozygous pups is significantly reduced at birth (highlighted in blue).

(B) Representative images of *miR-126⁺/⁺* and *miR-126⁻/⁻* littermate embryos and placentas at E12.5 and E15.5. Arrows indicate hemorrhaging in *miR-126⁻/⁻* embryos at E12.5 and arrow heads indicate systemic edema in *miR-126⁻/⁻* embryos at E15.5.

(C) Lengths (mm) and wet weights (mg) of embryos and placentas from *miR-126⁺/⁺* (n=7) and *miR-126⁻/⁻* (n=8) conceptuses at E12.5. Error bars indicate SEM.

(D) Lengths (mm) and wet weights (mg) of embryos and placentas from *miR-126⁺/⁺* (n=25) and *miR-126⁻/⁻* (n=6) conceptuses at E15.5. Error bars indicate SEM. (** p 0.01).
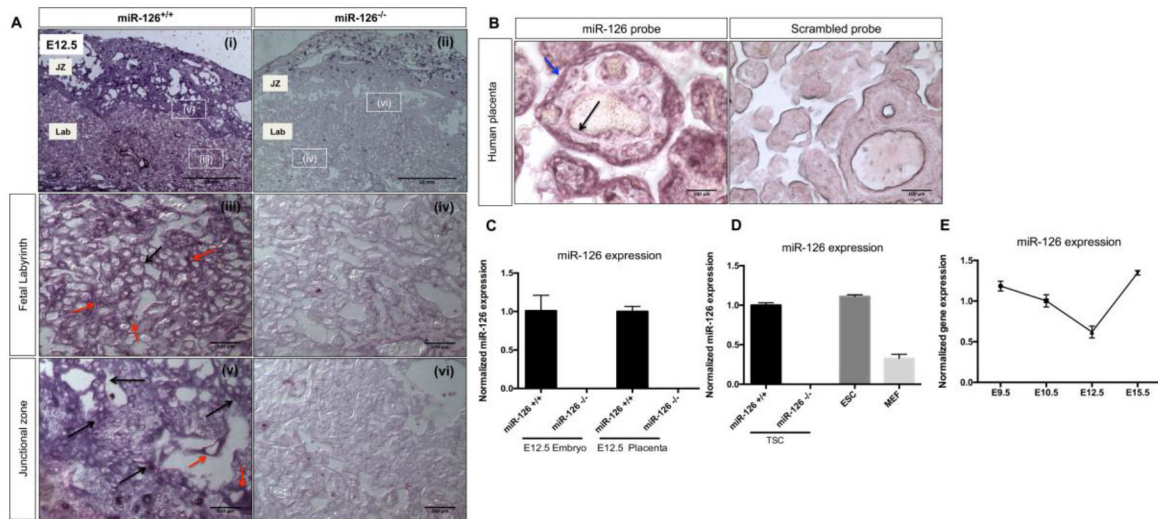
Figure 2: Trophoblasts and endothelial cells of murine and term human placentas express miR-126.

(A) (i) and (ii) Representative low magnification image of *miR-126⁺/⁺* (i) and *miR-126⁻/⁻* placentas (ii) stained with a DIG-labeled miR-126 LNA probe. Punctuate signal in panel (ii) are immune cells at the maternal-fetal interphase of the decidua. Lab: Fetal labyrinth, JZ: Junctional zone. Bar = 10 mm.

(iii) and (iv) Representative high magnification images of *miR-126⁺/⁺* (iii) and *miR-126⁻/⁻* (iv) placental fetal labyrinth stained with a DIG-labeled miR-126 LNA probe show miR-126 specific expression in the fetal labyrinth in endothelial cells (black arrow) and syncytial trophoblasts (red arrow) of *miR-126⁺/⁺* placentas (iii). No detectable miR-126 expression in the fetal labyrinth of *miR-126⁻/⁻* placentas (iv). Bar = 100μm.

(v) and (vi) Representative high magnification images of *miR-126⁺/⁺* (iii) and *miR-126⁻/⁻* (iv) placental junctional zones stained with a DIG-labeled miR-126 LNA probe. miR-126 specific expression in the junctional zone in trophoblast giant cells (red arrow), spongiotrophoblasts and glycogen trophoblasts (black arrow) of *miR-126⁺/⁺* placentas (v). No detectable miR-126 expression in the junctional zone of *miR-126⁻/⁻* placentas (vi). Bar = 100μm.
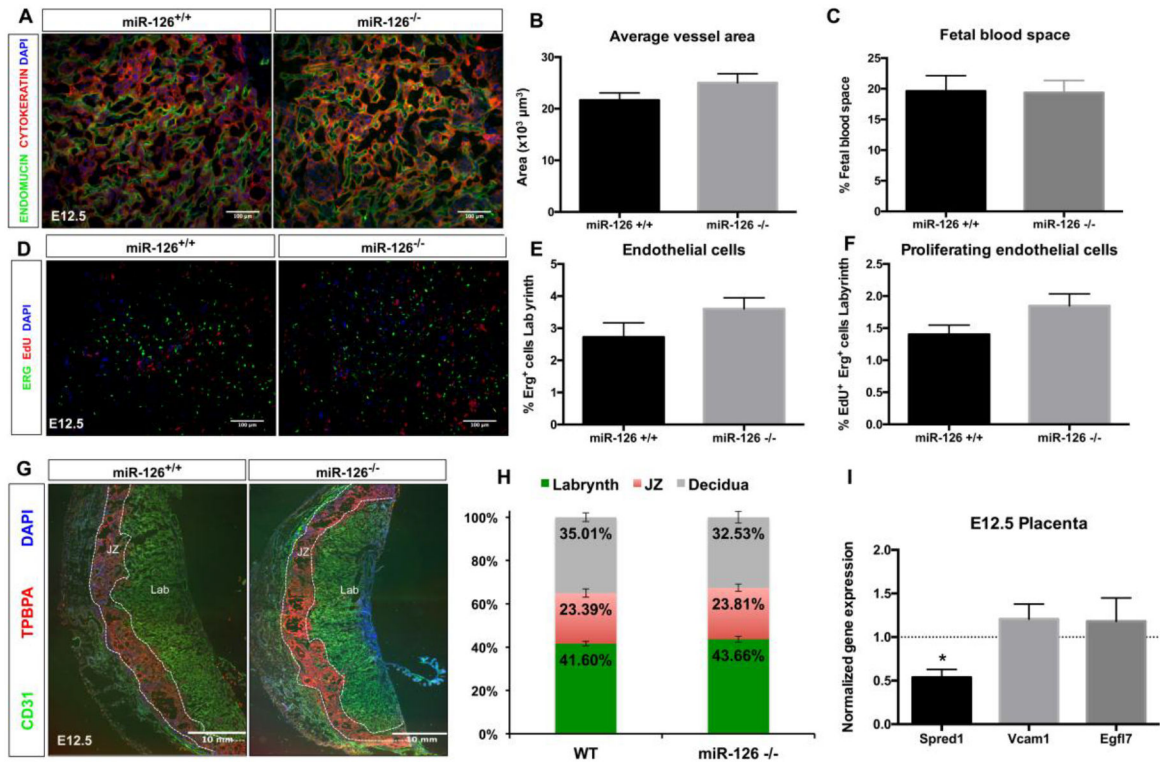
(B) Representative images of human term placenta sections hybridized with a DIG labeled miR-126 LNA probe (left panel), or a DIG-labeled scrambled LNA probe (right panel). miR-126 specific expression in the syncytiotrophoblasts (blue arrow) and fetal endothelial cells (black arrow) in sections hybridized with the DIG-labeled miR-126 LNA probe, but not in sections hybridized with the DIG-labeled scrambled LNA probe. Bar = 100μm.

(C) Quantification of miR-126 expression in *miR-126⁺/⁺* (n=3) and *miR-126⁻/⁻* (n=3) embryos and placentas at E12.5 by quantitative RT PCR. Error bars indicate SEM. Expression levels normalized to levels in *miR-126⁺/⁺* embryos.

(D) Quantification of miR-126 levels in *miR-126⁺/⁺* and *miR-126⁻/⁻* trophoblast stem cells (TSC), embryonic stem cells (ESC) and mouse embryonic fibroblasts (MEF) by quantitative RT PCR (n=3 each; technical replicates). Expression levels normalized to levels in *miR-126⁺/⁺* TSCs. Error bars indicate SEM.

(E) Quantification of miR-126 expression in placentas at E9.5, E10.5, E12.5, E15.5 by quantitative RT PCR (n=4). Error bars indicate SEM.

Figure 3: *miR-126*−/− placentas do not display overt vascular phenotypes at E12.5

(A) Representative images of the fetal labyrinth from E12.5 *miR-126*+/+ and *miR-126*−/−
placentas immunostained with antibodies against ENDOMUCIN to mark the fetal
endothelium of the labyrinth and CYTOKERATIN to mark trophoblasts.

(B) Quantification of the average area of fetal vessels in the fetal labyrinth of *miR-126*+/+
(n=4) and *miR-126*−/− (n=4) placentas. Error bars indicate SEM.

(C) Quantification of fetal blood space cells in the fetal labyrinth zone of *miR-126*+/+ (n=4)
and *miR-126*−/− (n=4) placentas.

(D) Representative images of E12.5 *miR126*+/+ and *miR-126*−/− placentas immunostained
with an ERG antibody to mark the fetal endothelium of the labyrinth and EdU to mark
proliferating cells (ClickiT chemistry).

(E) Quantification of ERG+ endothelial cells in the fetal labyrinth zone of *miR-126*+/+ (n=4)
and *miR-126*−/− (n=4) placentas. Error bars indicate SEM.

(F) Quantification of EdU+ ERG+ proliferating endothelial cells in the fetal labyrinth zone of
miR-126+/+ (n=4) and *miR-126*−/− (n=4) placentas. Error bars indicate SEM.

(G) Representative images of E12.5 *miR-126*+/+ and *miR-126*−/− placentas immunostained
with antibodies against CD31 to mark the endothelium of the labyrinth (Lab) and maternal
arteries and TPBPA to mark trophoblasts of the junctional zone (JZ). Bar = 100mm.

(H) Quantification of the areas of the fetal labyrinth (CD31, green), junctional zone (Tpbpa,
red) and the decidua (gray) as a fraction of the total area (fetal labyrinth+ junctional zone +
decidua) of *miR-126*+/+ (n=4) and *miR-126*−/− (n=4) placentas (3 sections 100μm apart at
the placental midline). Error bars indicate SEM.

(I) Gene expression levels of direct targets of miR-126, Vcam-1 and Spred-1, and of Egfl7.
Expression level in E12.5 *miR-126*+/+ placentas for each gene is normalized to 1.
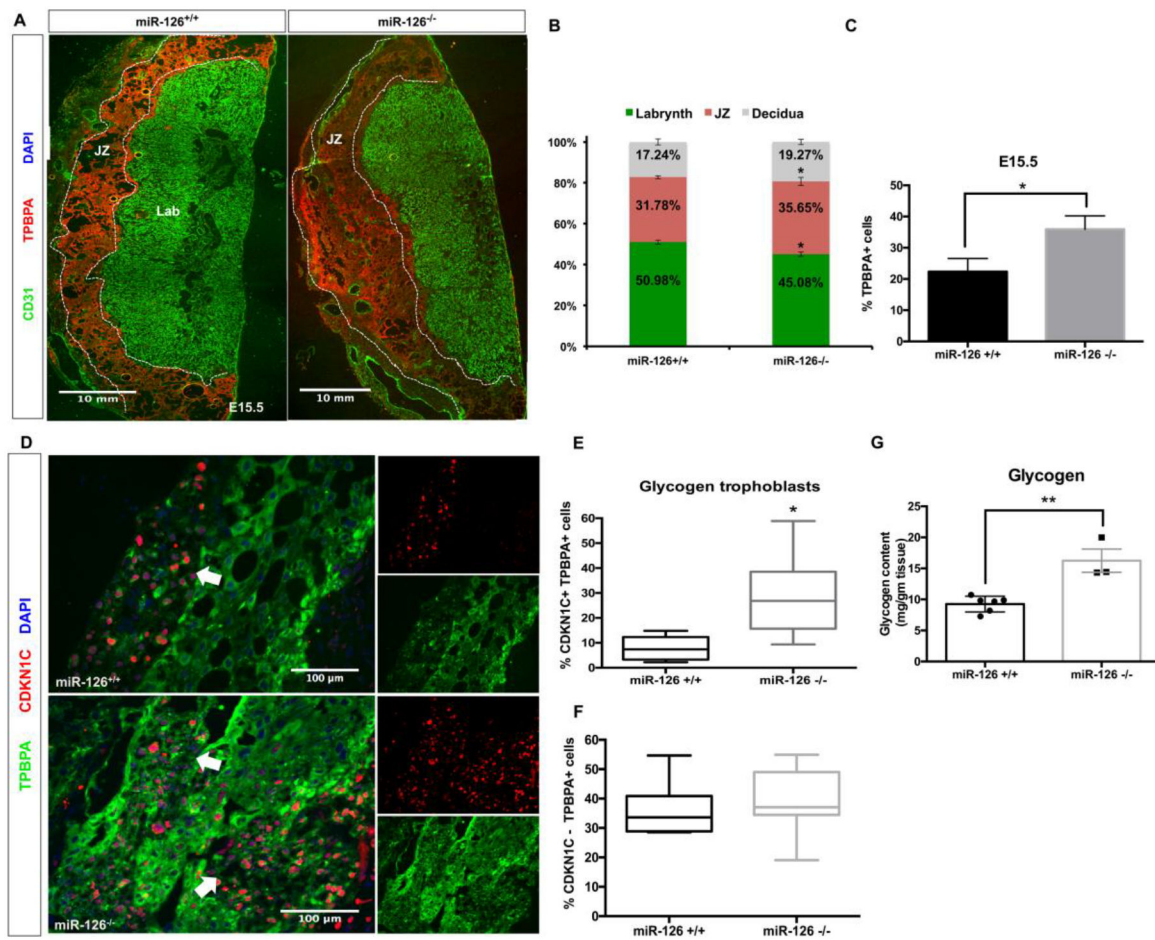
Figure 4: Hyperplasia of the junctional zone from increased numbers of glycogen trophoblasts in *miR-126^(−/−)* placentas at E15.5

(A) Representative images of E15.5 *miR-126^(+/+)* and *miR-126^(−/−)* placental sections, immunostained with antibodies against CD31 (green) to mark the endothelium of the labyrinth (Lab) and maternal arteries, and TPBPA (red) to mark trophoblasts of the junctional zone (JZ). Dotted white lines indicate the junctional zone/labyrinth and junctional zone/decidua boundaries.

(B) Quantification of the areas of the fetal labyrinth (CD31, green), junctional zone (TPBPA, red) and the decidua (gray) as a fraction of the total area (fetal labyrinth+ junctional zone+ decidua) of *miR-126^(+/+)* (n=6) and *miR-126^(−/−)* (n=5) placentas (4 sections from each placenta, 100μm apart at the placental midline). Error bars indicate SEM. (* p 0.05).

(C) Quantification of TPBPA^+ cells in *miR-126^(+/+)* (n=6) and *miR-126^(−/−)* (n=5) placentas at E15.5, shown as a percentage of total TPBPA^+ cells in placental sections. Error bars indicate SEM (* p 0.05).

(D) Representative immunofluorescence images of sections from *miR-126^(+/+)* and *miR-126^(−/−)* E15.5 placentas co-immunostained with a CDKN1C antibody to mark glycogen trophoblast cells and a TPBPA antibody to mark junctional zone trophoblasts. Arrows indicate clusters of CDKN1C^+TPBPA^+ glycogen trophoblast cells in the junctional zone. Bar = 100μm.

(E) Quantification of CDKN1C$^+$TPBPA$^+$ glycogen trophoblast cells in the junctional zone of *miR-126$^{+/+}$* (n=4) and *miR-126$^{-/-}$* (n=3) placentas. Data are shown as percent of total number of CDKN1C$^+$TPBPA$^+$ cells in each image. Error bars indicate SEM (* p 0.05).

(F) Quantification of CDKN1C$^-$TPBPA$^+$ spongiotrophoblasts in the junctional zone of *miR-126$^{+/+}$* (n=4) and *miR-126$^{-/-}$* (n=3) placentas. Data are shown as percent of total number of cells in each image. Error bars indicate SEM.

(G) Quantification of glycogen content (mg glycogen per gram tissue) in *miR-126$^{+/+}$* (n=6) and *miR-126$^{-/-}$* (n=3) placentas. Error bars indicate SEM. (** p 0.01).
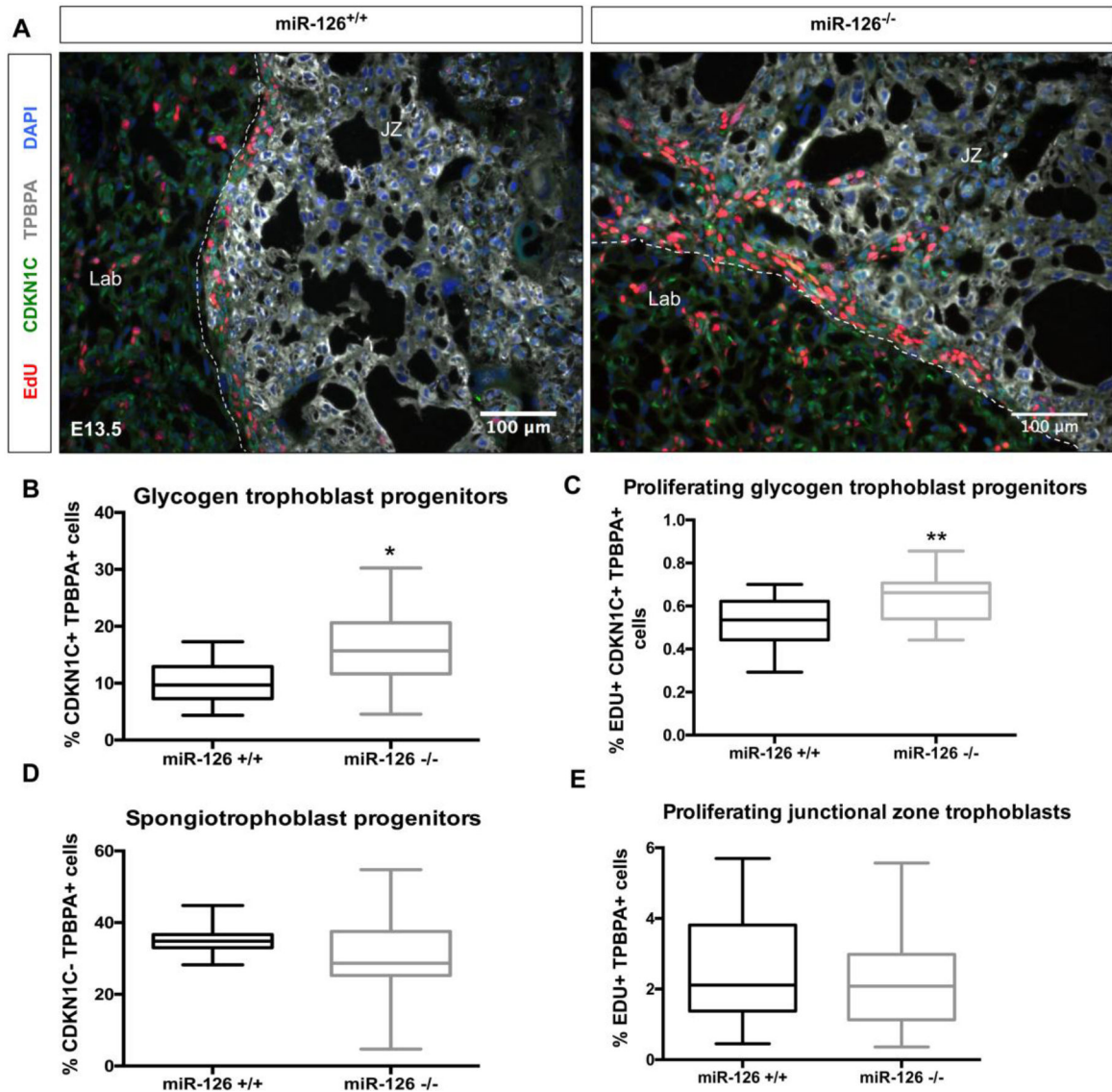
Figure 5: Increased numbers of proliferating glycogen cells in E13.5 *miR-126⁻/⁻* placentas at E13.5.

(A) Representative images of sections of *miR-126^{+/+}* and *miR-126^{−/−}* placentas at E13.5, immunostained with CDKN1C antibody, TPBPA antibody and EdU (ClickiT chemistry). Dotted white line indicates the boundary between the junctional zone and labyrinth. Bar = 100μm.

(B) Quantification of CDKN1C⁺TPBPA⁺ glycogen trophoblasts in the junctional zone of *miR-126^{+/+}* (n=4) and *miR-126^{−/−}* (n=4) placentas. Data are shown as percent of total number of CDKN1C⁺TPBPA⁺ cells in each image. Error bars indicate SEM. (* p 0.05).

(C) Quantification of EdU⁺CDKN1C⁺TPBPA⁺ proliferating glycogen trophoblast progenitor cells in the junctional zone of *miR-126^{+/+}* (n=4) and *miR-126^{−/−}* (n=4) placentas. Data are shown as percent of EdU⁺CDKN1C⁺TPBPA⁺ cells out of total number of cells in each image. Error bars indicate SEM. (** p 0.01).

(D) Quantification of CDKN1C⁻TPBPA⁺ spongiotrophoblasts in the junctional zone of *miR-126⁺/⁺* (n=4) and *miR-126⁻/⁻* (n=4) placentas. Data are shown as percent of total number of CDKN1C⁻TPBPA⁺ cells in each image. Error bars indicate SEM.

(E) Quantification of EdU⁺TPBPA⁺ proliferating cells in the junctional zone of *miR-126⁺/⁺* (n=4) and *miR-126⁻/⁻* (n=4) placentas. Data are shown as percent of total number of EdU⁺TPBPA⁺ cells in each image. Error bars indicate SEM.
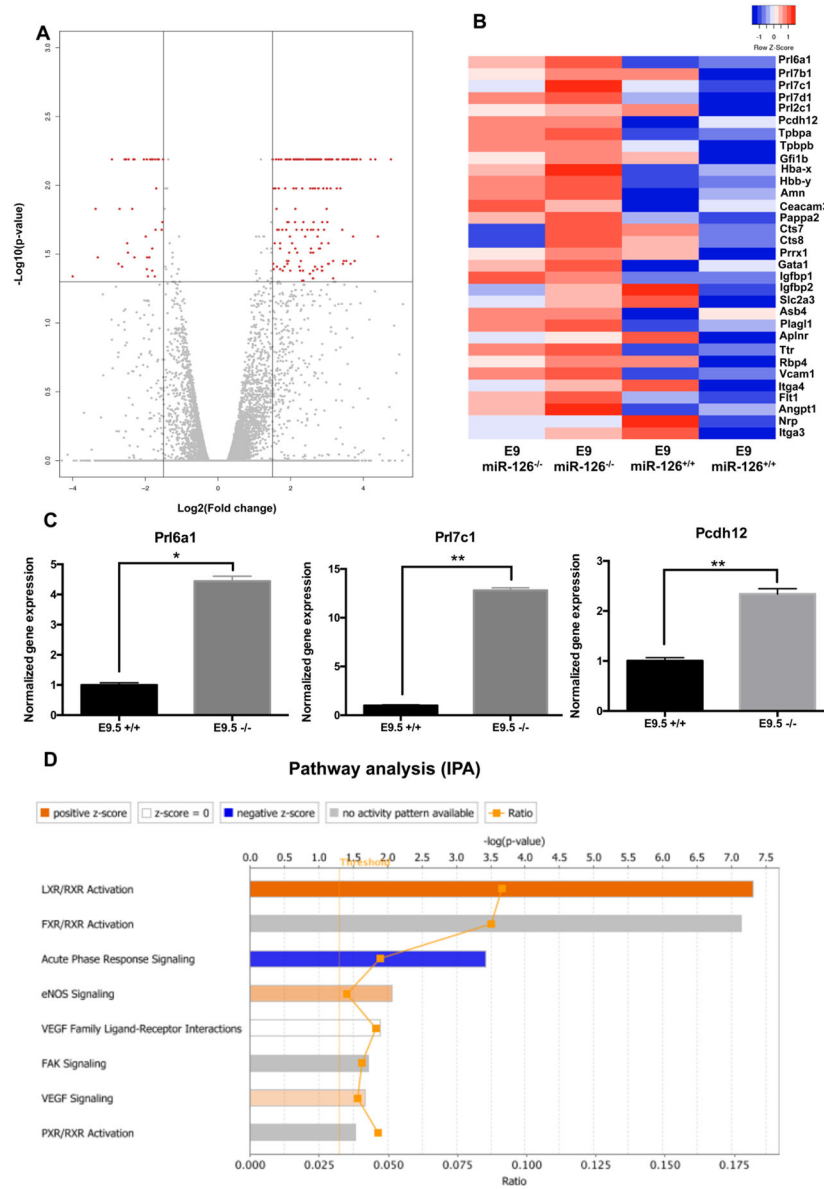
Figure 6: Increased expression of GlyT-specific prolactin genes in early *miR-126⁻/⁻* placentas

(A) Transcriptome of E9.5 *miR-126⁻/⁻* placentas when compared to *miR-126⁺/⁺* placentas. X-axis represents logarithm to base 2 of fold-changes and y-axis represents negative logarithm to the base 10 of the p-values. Filtering criteria of fold-change = ±2 and p value 0.05 are used. Horizontal black line indicates the p value cut-off. Blue dots represent transcripts with ±2 fold change with p value > 0.05. Orange dots represent transcripts significantly dysregulated in *miR-126⁻/⁻* placentas when compared to *miR-126⁺/⁺* placentas (fold-change = ±2 and p value 0.05).

(B) Heat map showing expression of selected dysregulated genes in E9.5 *miR-126⁻/⁻* and *miR-126⁺/⁺* placentas. Log-transformed expression values are represented with upregulated genes in shades of red and downregulated genes in blue. Several GlyT specific prolactin

genes are significantly upregulated. Several genes regulating metabolism and angiogenesis are also significantly upregulated.

(C) qRT-PCR analysis showing fold change expression of GlyT specific prolactin genes *Prl6a1*, *Prl7c1* and the protocadherin gene *Pcdh12* from E9.5 *miR-126^{-/-}* and *miR-126^{+/+}* placentas. (n=4, from two litters for each genotype). Error bars indicate SEM. (* p 0.05) (** p 0.01)
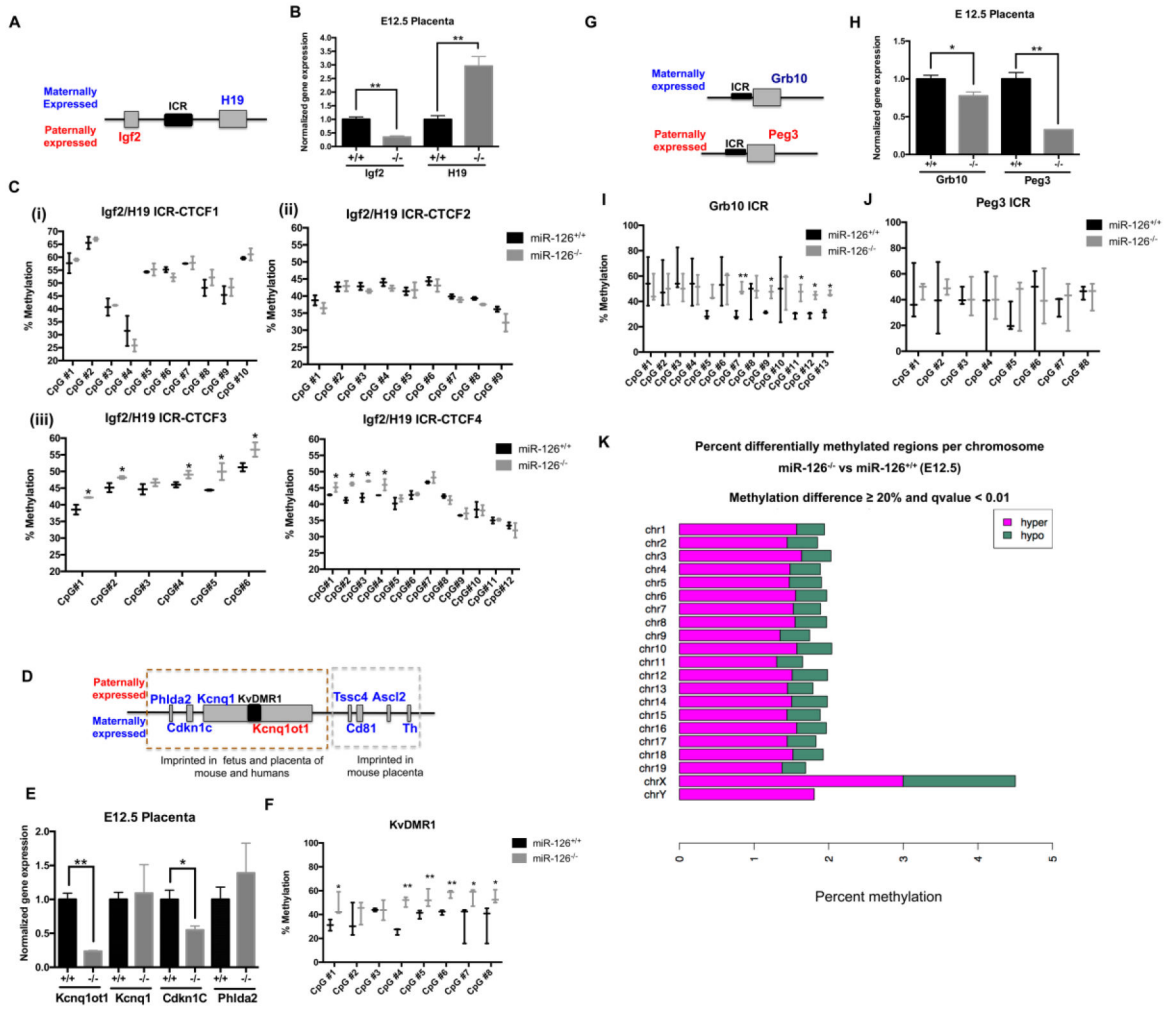
Figure 7: *miR-126* affects expression of imprinted gene specifically in the placenta.

(A) Schematic representation of the *Igf2/H19* imprinted cluster and its imprint control center (ICR) upstream of *H19*.

(B) Gene expression levels of paternally expressed gene *Igf2* and maternally expressed non-coding RNA H19 in E12.5 placentas by quantitative RT PCR (n=4, from two litters for each genotype). Error bars indicate SEM. (** p 0.01).

(C) Percent methylation of CpGs at CTCF binding sites CTCF1 (i), CTCF2 (ii), CTCF3 (iii) and CTCF4 (iv) at the ICR. Bars indicate minimum and maximum values. (* p 0.05)

(D) Schematic representation of the *Kcnq1ot1* imprinted cluster and the imprint control center KvDMR1 at the promoter of *Kcnq1ot1*.

(E) Gene expression levels of paternally expressed non-coding RNA Kcnq1ot1 and maternally expressed genes *Kcnq1*, *Cdkn1C* and *Phlda2* in E12.5 placentas by quantitative RT PCR (n=4, from two litters for each genotype). Error bars indicate SEM. (** p 0.01) (* p 0.05)

(F) Percent DNA methylation of CpGs at the KvDMR1 imprint control center. Bars indicate minimum and maximum values. (** q 0.01) (* q 0.05)

(G) Schematic representation of imprinted genes *Grb10* and *Peg3* and imprint control centers at their respective promoters.

(H) Gene expression levels of maternally expressed gene *Grb10* and paternally expressed *Peg3* and in E12.5 placentas by quantitative RT PCR (n=4, from two litters for each genotype). Error bars indicate SEM. (* p 0.05)

(I) Percent DNA methylation of CpGs at the *Grb10* imprint control center. Bars indicate minimum and maximum values. (** q 0.01) (* q 0.05)

(J) Percent DNA methylation of CpGs at the *Peg3* imprint control center. Bars indicate minimum and maximum values.

(K) Percentage of differentially methylated CpG rich regions with a significantly increased methylation of 20% in *miR-126⁻/⁻* placentas (n=3) when compared to *miR-126⁺/⁺* placentas (n=3). Methylation difference 20% and q value 0.01.